Astron. & Astrophys. 12, 297–309 (1971)

On the Computation of Shock Heated Models for the Solar Chromosphere and Corona

P. Ulmschneider
Astronomisches Institut und Sternwarte der Universität Würzburg

Received January 4, 1971

Theoretical models are computed for the chromosphere and corona starting at a height of 800 km. The observational chromospheric models can be reproduced very well up to 1400 km assuming weak shock waves with periods of around 27 s. At greater heights the Hα and Lyman continuum radiation loss regions can presently not be treated adequately. The observed Lyα and XUV line fluxes are used to extend the theoretical model computation into the transition region and lower corona. Acoustic waves of periods between 100 and 200 s are shown to develop into strong shocks in the lower corona. The heating of these waves determines the theoretical models up to the coronal temperature maximum.

The notion that short period waves of around 27 s heat the chromosphere while long period waves of around 100 to 200 s heat the corona was found to be consistent with the acoustic wave fluxes and frequencies of spectra given by Stein (1968).

Key words: shock heating — chromosphere — corona

1. Introduction

In recent years increasingly reliable chromospheric models derived from eclipse as well as UV and sub mm observations were published (Thomas and Athay,1961; Gingerich and de Jager, 1968; Athay, 1969; Noyes and Kalkofen, 1970; Gingerich *et al.*, 1971). On the other hand theoretical computations of Uchida (1963), Kuperus (1965), Ulmschneider (1967), Kopp (1968) and de Loore (1970) show that models of the outer atmosphere of stars may be constructed on a purely theoretical basis. Similarly to the computation of model atmospheres for the photospheric layers one hopes to compute models of the chromosphere and corona for an arbitrarily given star. However this problem is still far from a satisfactory solution. The reason for this is the fact that the physics of the outer layers of a star is much more complicated than in a typical stellar atmosphere problem and more-over escaped observation until recent advances in UV and sub mm techniques.

First the question of the heating mechanism is still not settled satisfactorily. There is strong evidence for the current opinion that dissipation of waves emanating from the convection zone is the dominant heating mechanism for the chromosphere and corona. This does not mean however that other mechanisms can be completely excluded. But even granted the shock heating mechanism the uncertainty is very large of how much mechanical flux ultimately is available to heat the chromosphere and how to compute it from a given convective stellar atmosphere. Ulmschneider (1970) has shown that possibly more than 90 percent of the sound energy generated in the convection zone might be lost by radiation before this energy is available for chromospheric heating.

Second there is the question of space and time dependence. Observations in white light or Hα show a multitude of transient and space dependent phenomena on the solar surface. Further outward towards the corona, radio and XUV observations show the sun only in certain hot spots. Therefore the question arises up to what height the sun is still representable by a one dimensional depth variable and from what height upwards we do need three or more variables to characterize the atmosphere.

Third the question of radiation loss is vastly more complicated than in a typical stellar atmosphere problem. Aside from chromospheric H^- loss the Lyman continuum, the Lyman and Balmer lines must be treated with a full non-LTE method. This means that the radiation loss which sensitively balances shock heating and thermal conduction at every point is not dependent on the local values of temperature and pressure but depends in a complicated way on the atmosphere as a whole. This is complicated

even more by the inhomogeneous structure of the atmosphere.

Nevertheless significant progress can be made by tackling one problem at the time. In the lower chromosphere, extending over the region from the temperature minimum to the onset of the transition layer where the temperature in a few scale heights jumps to essentially coronal temperatures, the radiative loss can be fairly well (Athay, 1966) represented by the predominant contributor, the H^- continuum loss. This loss might be treated in LTE and therefore easily computed as a function of temperature and pressure at every height. With the assumption of only a variation with height and using the shock heating mechanism a chromospheric model may be computed by balancing in the energy equation heating against radiative losses. This model is valid as long as H^- is the main source of radiative loss. It can be brought into close agreement with recent observational chromospheric models with very reasonable assumptions about mechanical energy fluxes and frequencies of the shock waves.

Extending the model of the lower chromosphere further upwards we enter the non-LTE hydrogen emission region. Although a program to compute the non-LTE radiation loss on basis of a given temperature and pressure versus height relation was kindly given to me by W. Kalkofen of the S.A.O. the question of how to correct temperature and pressure to balance heating and cooling was too difficult to answer. It was thus necessary to approximate the hydrogen radiation loss values derived from observation of the Lyα and Ly continuum fluxes of the sun. With this it was possible to extend the model into the lower corona. The extension to the maximum of the coronal temperature was made by considering the balance of the heating mechanism which consists here of strong shock waves and the main cooling mechanism which is thermal conduction.

Models computed this way necessarily are not able to predict any inhomogeneous structure but may serve to give an idea of the average behavior of temperature and pressure along a streamer and finally give insight into what problems must be tackled next to improve our knowledge of how to compute models for an outer stellar atmosphere.

2. Heating Mechanism

A. Acoustical Wave Flux

All recent chromospheric models show after a minimum of the temperature (at about 550 km above $\tau_{5000} = 1$, Gingerich *et al.*, 1971) a rise of temperature which is thought to be caused mainly by the dissipation of compressional waves. This was first suggested by Biermann (1946). However the dissipation of these waves which, as is fairly certain by now are sawtooth type shock waves (Kuperus, 1969), is by no means the only mechanism to increase the temperature minimum.

Both the Cayrel mechanism and line blanketing (Athay, 1970) may increase the temperature after the temperature minimum considerably as a consequence of the conservation of radiative flux. Nevertheless one expects that a few hundred km past the temperature minimum mechanical heating will certainly be the sole cause for the temperature rise.

An important fact as it turns out is that the compressional waves which are produced in the convection zone do not arrive as a monochromatic wave but rather arrive in form of a frequency spectrum with a bandwidth of about two orders of magnitude. Stein (1968) has computed frequency spectra of acoustic waves produced in the convection zone based on various theoretical assumptions. For an exponential space spectrum with an exponential frequency factor (EE spectrum) of the turbulence he finds a maximum flux at a period of 38 s. The region where the flux is 10 percent of the maximum value extends from 16 s to more than 210 s. The total flux integrated over frequency is $\pi F_{\text{Mech}} = 9.9 \times 10^7$ erg/cm^2 s. For the Spiegel spectrum with an exponential frequency factor (SE spectrum) he found 29 s for the maximum and 8 s to 157 s for the band width. The total flux is $\pi F_{\text{Mech}} = 5.5 \times 10^7$ erg/cm^2 s. For an exponential space spectrum with a gaussian frequency factor (EG spectrum) a maximum of 81 s and 35 s to 393 s for the band width was found. The flux $\pi F_{\text{Mech}} = 7.2 \times 10^6$ erg/cm^2 s for this spectrum is quite low and most likely not sufficient to balance the radiative loss of chromosphere and corona of about 3×10^6 erg/cm^2 s (Ulmschneider, 1970). It seems therefore reasonable to disregard this spectrum.

Propagating outward towards the temperature minimum the acoustic waves are focused by the decreasing index of refraction into predominantly vertical direction. Through the temperature minimum only those waves whose frequency is above the cut-off frequency are allowed to pass. The cut-off frequency is (Hines, 1960, p. 1466)

$$\nu_a = \frac{\gamma g}{4\pi c} . \qquad (1)$$

Here γ is the ratio of specific heats, g the gravitational

acceleration and c the sound velocity. With $c = 6.7 \times 10^5$ cm/s for a temperature of $T_0 = 4200°$ K we have $P_a = 1/\nu_a = 184$ s. This shows that both the EE and the SE spectra are easily transmitted.

As Eq. (1) was derived under the assumption of linearized equations we have to check whether indeed e.g. the density perturbation ϱ' of the wave is small against the equilibrium density ϱ_0 of the atmosphere. The flux of acoustic waves may be written (Landau, Lifshitz, 1959, p. 250)

$$\pi F_{\text{Mech}} = \varrho_0 c^3 \left(\frac{\varrho'}{\varrho_0}\right)^2 . \tag{2}$$

With $\varrho_0 = 3.5 \times 10^{-9}$ g/cm^3 and $c = 6.7 \times 10^5$ cm/s we find $\varrho_0 c^3 = 1.1 \times 10^9$ erg/cm^2 s. As we have seen above the total mechanical fluxes of the EE and SE spectra are far below this value, which is even more so as radiative losses will have substantially decreased the total mechanical flux at this height. It is thus entirely justified to use the linear theory result.

Summing up we may conclude that a large source of acoustical energy is available and this energy is expected to reach the chromosphere. There is however the question of how much energy remains to heat the chromosphere and corona and in what form this heating is actually done.

An acoustic wave travelling outward into the optically thin region towards the temperature minimum will suffer besides negligible amounts of viscous losses strong radiative losses. An idea of the importance of these losses in the upper photosphere may be obtained by computing the radiative relaxation time T_R, that is the time after which a temperature difference of ΔT would cool to zero if the cooling rate were constant.

$$T_R = \frac{c_p \Delta T}{4\pi(j - j_0)} = \frac{5/2\, R/\mu}{16 \bar{\varkappa} \sigma T^3} . \tag{3}$$

Here $c_p = 5/2\, R/\mu$ is the specific heat, j the emission coefficient, $\bar{\varkappa}$ the Rosseland mean opacity and σ the Stefan-Boltzmann constant. Table 1 gives values for T_R for $\Delta T = 1°$ K as given by Noyes and Leighton (1963). Note that instead of c_v we took here c_p because temperature perturbations are expected to cool in pressure equilibrium with the surroundings.

How much energy this radiative loss ultimately takes out of the wave can only be answered by a detailed time dependent computation. However, by the amount of radiative flux produced by chromosphere and corona after the temperature minimum which is roughly 3×10^6 erg/cm^2 s (Ulmschneider, 1970) only 3 to 5 percent of the original flux finally arrive to balance the energy losses of the higher layers.

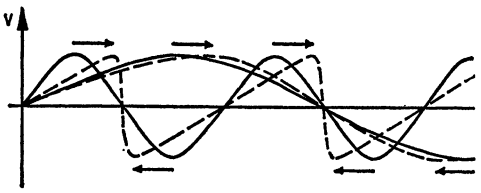

Fig. 1. Profile distortions of sinusoidal waves with different frequencies but identical initial flux after the same time interval. It is seen that the high frequency wave developes into a shock wave much more rapidly

Table 1. *Radiative relaxation time T_R as function of height after Noyes and Leighton (1963) multiplied by 5/3*

τ_{5000}	height (km)	T_R (s)
1	0	1.6
0.1	140	16
0.01	260	58
0.001	396	167

B. Shock Wave Formation and Heating of the Chromosphere

Decreasing radiative losses force the acoustic density and velocity perturbations to grow because of energy conservation and as compression waves travel faster than expansion waves the profile distorts and forms a shock wave. In this process the frequency of the wave is not altered and a sawtooth profile results.

The height at which the shock wave is fully developed depends on the initial mechanical flux and on the radiative losses. Of greatest importance for the heating of the outer solar atmosphere is however the fact that the height of shock formation depends sensitively on the frequency of the acoustic wave. High frequency waves form shocks at considerably shorter space distances than low frequency waves.

This can be seen as follows. Consider waves of different frequency but identical initial flux. Because e.g. the velocity perturbation v is for a given flux (Eq. (2)) independent of frequency, the profiles of the waves distort at every frequency with the same rate according to the equation (Landau and Lifshitz, 1959, p. 373)

$$u = c + \frac{1}{2}(\gamma + 1)\, v , \tag{4}$$

where u is the total velocity at a point in the wave. The effect of this equal rate of profile distortion on a sinusoidal profile is shown in Fig. 1. In the high frequency wave the profile distorts to almost a shock wave because of the short wavelength. For the low frequency wave the same profile distortion does not appreciably alter the sinusoidal wave form.

Let us consider the EE or SE flux spectra. We would expect the high frequency part of the spectrum to develop into shocks earlier than the low frequency part by a considerable height interval. If we suppose the region before the temperature minimum to be dominated by radiative losses (Table 1) such that no shock waves are able to develop we may obtain an estimate of the height of shock formation using the results of a nonlinear computation of Bird (1964). He shows for an atmosphere with a constant positive temperature gradient of 33 K/km and an initial sound velocity of 6 km/s that an acoustic wave of 300 s period starts to form a shock discontinuity after 1100 km while transforming into a fully developed wave at a considerably greater distance. This case is for a flux at the temperature minimum of 2×10^7 erg/cm^2 s (with $\varrho_0 = 3.5 \times 10^{-9}$ g/cm^3) which is very large. In the case with a flux of 2×10^6 erg/cm^2 s which is probably too low the shock formation distance is 4000 km. The shock formation distances are found to be proportional to the wave period P. If we assume a wave period of roughly one tenth of Bird's value we obtain a distance of 110 to 400 km or about the height of 700 to 800 km in the model of Gingerich *et al.* (1971). The assumption of shock heating shortly after the temperature minimum is therefore entirely consistent with what we expect for the height of shock formation of high frequency waves and with the frequencies offered by the SE and EE spectra.

Because in the SE and EE spectra the initial wave fluxes of the very high frequencies are (periods of about 8 to 20 s) quite small and thus their height of shock formation is great, we expect a mean frequency between the maximum and the short end of the frequency band to first develop into a shock wave. This would be between 20 and 38 s for the EE spectrum and between 20 and 29 s for the SE spectrum. Ulmschneider (1970) compared radiative losses computed on basis of empirical solar models with the dissipation of shock waves of different flux and frequency. It is encouraging that he was able to conclude that radiative losses could be balanced by shock dissipation only by assuming a wave period of around 10 s. In the present work wave periods of between 25 and 30 s are found in comparison with the newest empirical solar models (see Fig. 2).

Summing up we may conclude that the heating mechanism for the chromosphere up to the transition layer is probably the dissipation of weak (because of the flux) sawtooth type shock waves with a period of around 30 s with an uncertainty of about a factor of 1.5. Because more and more lower frequencies develop into shocks we expect a lowering of the frequency of the shock waves with increasing height.

C. Heating of the Corona

The question of heating of the corona is less well understood than the heating of the chromosphere. The low frequency part of the EE and SE spectra as we have seen in Bird's (1964) computation will develop into shock waves at considerable heights. Radiative losses will aside from the losses before the temperature minimum be probably of some – possibly minor – influence in the Balmer emission region. The Lyman emission however is balanced by thermal conduction such that very little of the observed flux is due to a direct wave loss. We expect thus that the wave which penetrates the Lyman region of roughly 10 km in about 1 s suffers very little radiation losses. In Table 2 we have computed the strength $\bar{\eta}$ of a shock wave of 3×10^5 erg/cm^2 s which is a lower estimate of the radiation flux of the transition layer and corona due to Lyα and all other emitters. This flux is certainly an underestimate of the actual mechanical flux needed to eventually balance the radiation flux because also strong flux losses occur in order to balance reflection (see Fig. 5). For the definition of $\bar{\eta}$ see Eq. (6).

We invariably find (and with inclusion of reflection even more so) that the shock waves are strong, justifying previous strong shock computations of Kuperus (1965), Ulmschneider (1967), Kopp (1968). This is what we expect from a wave which loses little energy by radiation. Finally let us consider that only

Table 2. *Strength $\bar{\eta}$ of a shock wave which carries a flux of* 3×10^5 erg/cm^2 s *in the corona. The strength $\bar{\eta}$ indicates strong shock waves*

T (°K)	c (cm/s)	p (dyn/cm^2)	$\bar{\eta}$
$1.2 \cdot 10^5$	$5.2 \cdot 10^6$	$1.1 \cdot 10^{-1}$	1.96
$4.2 \cdot 10^5$	$9.6 \cdot 10^6$	$1.1 \cdot 10^{-1}$	1.45
$8.9 \cdot 10^5$	$1.4 \cdot 10^7$	$1.1 \cdot 10^{-1}$	1.21
$1.6 \cdot 10^6$	$1.9 \cdot 10^7$	$1.1 \cdot 10^{-1}$	1.05

about 1 percent of the initial mechanical flux (1/2 total flux) produced in the convection zone is needed to heat the corona and transition layer.

What wave periods do we expect for coronal shock waves? First it is clear that waves which develop into shocks in the chromosphere cannot be considered as heating agents of the corona, as when a shock is developed, the wave loses energy very rapidly. Second because the shock formation distance is proportional to the period, we expect all of the very short periods and a considerable part of the periods greater than 27 s to develop into shock waves in the chromosphere. Thus there remain for the corona periods of around 100 s with about an uncertainly of a factor of 2.

D. The Shock Equation

To determine the amount of mechanical heating one needs the shock equation which determines the amount of energy flux carried by the wave and how this varies as a consequence of dissipation and reflection. As we are at the moment unable to do a computation with an applied frequency spectrum we assume monochromatic waves representative for the chromosphere and corona.

For weak sawtooth shocks the mechanical flux may be written

$$\pi F_{\text{Mech}} = \frac{1}{12}\gamma\, p\, c\, \bar{\eta}^2\,, \tag{5}$$

where

$$\bar{\eta} = \frac{\varrho_2 - \varrho_1}{\varrho_1} < 1 \tag{6}$$

is the shock strength for weak shocks, ϱ_2 and ϱ_1 being the densities behind and in front of the shock discontinuity respectively. p is the gas pressure. The shock equation may then be written

$$\frac{d\bar{\eta}}{dh} = \frac{\bar{\eta}}{2}\left(-\frac{1}{\gamma}\frac{d\gamma}{dh} + \frac{\gamma g}{c^2} - \frac{3}{2c^2}\frac{dc^2}{dh} - \frac{(\gamma+1)\,\nu\,\bar{\eta}}{c}\right), \tag{7}$$

where ν is the frequency of the shock wave. The dissipation in erg/cm³ s may be given using

$$\frac{d\pi F_{\text{Mech}}}{dh} = -(\gamma+1)\frac{\bar{\eta}\nu}{c}\pi F_{\text{Mech}}\,, \tag{8}$$

while the energy loss due to reflection of the wave on its own temperature gradient is

$$\frac{d\pi F_{\text{Mech}}}{dh} = -\frac{1}{c^2}\frac{dc^2}{dh}\pi F_{\text{Mech}}\,. \tag{9}$$

For the derivation of these equations see Ulmschneider (1970). Equations (5), (8) and (9) may be combined to give

$$\frac{d\pi F_{\text{Mech}}}{dh} = -\frac{1}{c^2}\frac{dc^2}{dh}\pi F_{\text{Mech}} - \left(\frac{12(\gamma+1)^2}{\gamma p c^3}\right)^{1/2}\nu\,(\pi F_{\text{Mech}})^{3/2}\,. \tag{10}$$

In this equation the reflection term (first) and dissipation term (second) taking flux away from the wave are explicitly separated. As seen in Fig. 3 the reflection term due to the slow temperature gradient in the low chromosphere is always small (roughly 20 percent) against the dissipation term.

At this point we have to consider the recent work of Jordan (1970). He integrated the above equation in the chromosphere on the basis of recent empirical solar models using shock wave periods of 200 to 300 s. From the fact that at greater heights he always finds $\bar{\eta} > 1$ he concludes that shocks are always strong in the solar chromosphere. Assuming a fully developed shock wave of 200 to 300 s period at heights shortly behind the temperature minimum we could confirm Jordans finding of $\bar{\eta} > 1$ in our work. This is due to the fact as seen in Eq. (10) that because ν is small very little flux is taken out of the shock wave. The near flux conservation situation leads to a rapid growth of the wave amplitude, that is strength of the wave. However as shown above a wave of this frequency is very likely not developed before the transition region. Moreover Jordans general conclusion seems not valid for short period waves either. We have found in our work $\bar{\eta} < 1$ everywhere in the chromosphere for all periods less than 100 s. This indicates that Eq. (10) based on the assumption of weak shocks will be valid for computations in the chromosphere.

For the strong shock waves which are needed in the corona we may take the equations given by Ulmschneider (1967). For our computations here we may in first order neglect the influence of the solar wind and restrict ourselves to plane geometry.

The neglect of the solar wind in the region before the coronal temperature maximum may be justified as follows. At the earths orbit one observes an average ion flux of 8×10^8 ions/cm² s (Ness, 1968). At the solar surface we obtain from this a mass flux ϱu of 3×10^{-11} g/cm² s. With a particle density of 10^9 to 10^8 ions/cm³ we obtain a solar wind velocity u of between 1.5 and 0.15 km/s. Thus with a sound velocity c of 100 km/s the flow Mach number $M = u/c$ is very small.

We then have for the shock equation

$$\frac{dM_s}{dh} = \zeta\eta M_s\left(-\frac{\xi}{2c^2}\frac{dc^2}{dh} + \frac{(\zeta(\xi+\zeta)-1)g}{(\xi+\zeta)c^2} - \delta\frac{1}{\gamma}\frac{d\gamma}{dh}\right) - \frac{1}{4}\frac{\chi}{c\tilde{\mu}\tilde{\nu}}\,. \tag{11}$$

The flux of the strong shock wave is

$$\pi F_{\text{Mech}} = \nu(\phi - 1)\,\xi\, pc\,\tilde{\mu}\,\tilde{\nu} \tag{12}$$

and the dissipation rate

$$\frac{d\pi F_{\text{Mech}}}{dh} = -\frac{pv}{(\gamma-1)}\ln(\phi\theta^{-\gamma})\,. \tag{13}$$

Here M_s is the shock Mach number defined by

$$M_s = \frac{U}{c_1}\,, \tag{14}$$

where U is the velocity of the shock front and c_1 the sound velocity in front of the shock.

For weak shocks $M_s = 1 + \alpha$ where $\alpha < 1$.

The connection with $\bar{\eta}$ is given by

$$\bar{\eta} = \frac{4\alpha}{\gamma+1}\,. \tag{15}$$

For $\alpha \to 0$ the above equations reduce to the ones for weak shocks.

The quantities ϕ, θ, ξ are defined by

$$\phi = \frac{2\gamma M_s^2 - (\gamma-1)}{\gamma+1}\,, \tag{16}$$

$$\theta = \frac{(\gamma+1)M_s^2}{(\gamma-1)M_s^2+2}\,, \tag{17}$$

$$\xi = \frac{2M_s^2-2}{(\gamma+1)M_s}\,. \tag{18}$$

For $\delta, \zeta, \eta, \chi$ see Ulmschneider (1967), $\tilde{\mu}\,\tilde{\nu}$ is a shape factor.

In these equations the influence of reflection is not taken into account. It is convenient to integrate this shock equation and include reflection by writing an equation similar to Eq. (10) by eliminating M_s numerically out of Eqs. (13) and (12). For the shape factor $\tilde{\mu}\,\tilde{\nu}$ which for sawtooth waves is $P/12$ we take $P/6$ where P is the wave period. This is for the case that an acoustic wave develops into a strong shock wave with the compression part growing into a triangular shock and the expansion part being small.

From this we find

$$\pi F_{\text{Mech}} = \frac{2}{3}\,pc\,\frac{\gamma}{(\gamma+1)^2}\,\frac{(M_s^2-1)^2}{M_s} \tag{19}$$

which is solved for M_s and substituted into Eq. (13).

3. Radiative Loss Mechanisms

The radiative losses in the lower chromosphere are shown by Athay (1966) to be mainly due to the H^- ion and the Balmer series of hydrogen. The losses by the Lyman continuum and the strong radiative losses due to the Lyman lines of hydrogen govern the onset and lower part of the transition layer, while the upper transition layer and lower corona suffer radiation losses primarily from the lines of highly ionized metals. For the highest temperatures in the corona bremsstrahlung becomes more and more important.

A. H^- Losses

The total energy loss due to the H^- ion may be computed under the assumption of LTE (Athay, 1966; Ulmschneider, 1970) using the equation

$$\frac{d\pi F_{H^-}}{dh} = 4\pi\int_0^\infty (B_\nu(T) - B_\nu(T_0))\,K_\nu^{H^-}\,d\nu\,. \tag{20}$$

Here as usual B_ν denotes the Planck function, ν the frequency and $K_\nu^{H^-}$ the H^- absorption coefficient. The H^- absorption coefficient was computed with an approximation given by Gingerich (1964). As the H^- losses sensitively determine the temperature behavior of the chromospheric model the integral of Eq. (20) was computed rather accurately by doing a 64 Gauss integration cutting off the integration at a maximum frequency of

$$\nu_{\max} = 3.3 \times 10^{11}\,T\,. \tag{21}$$

For the boundary temperature T_0 a value of 4200° K was taken.

B. Balmer Series Losses

For the Balmer series losses Athay (1966b) has given an approximate formula

$$\frac{d\pi F_{Ba}}{dh} = \langle h\nu_{u2}\rangle\, N_2\, C_{23}\,. \tag{22}$$

Here N_2 is the number density of hydrogen atoms in the second level, C_{23} the rate of collisional excitation from the second to the third level and $\langle h\,\nu_{u\,2}\rangle = 4.0 \times 10^{-12}$ is a mean energy of the Balmer series. C_{23} was computed using the BOW cross section (Burke *et al.*, 1967). We have

$$C_{23} = N_e\, 4\pi a_0^2 \left(\frac{8k}{\pi m_e}\right)^{1/2}\sqrt{T}\,\frac{f_{23}}{(\gamma_{23})^2} \cdot U_{23}(E_1(U_{23}) + 0.148\,U_{23}\,E_5(U_{23}))\,, \tag{23}$$

where $U_{23} = E_H \gamma_{23}/kT$, $\gamma_{23} = 5/36$, $f_{23} = 0.6407$ is the absorption oscillator strength, N_e the electron density, E_1 and E_5 are exponential integral functions and the rest of the symbols have their usual meaning.

For a given temperature and pressure one can easily compute N_2^*, the LTE value of the number density. But in conditions out of LTE we have

$$N_2 = b_2 N_2^* \tag{24}$$

with b_2 differing substantially from the LTE value 1. Noyes and Kalkofen (1970) have shown that b_2 varies from 1.56 at a height of 801 km over $\tau_{5000} = 1$ to 183 at a height of 1865 km in their empirical solar model based on Lyman continuum observations. There is no way of knowing b_2 beforehand as it is determined by the temperature structure of the atmosphere as a whole.

The point-dashed line in Fig. 2 shows the result of computations with $b_2 = 1$ in comparison with the observed temperature versus height relation of Noyes and Kalkofen (1970). It is seen that the computed temperature gradient becomes increasingly smaller relative to the observed temperature gradient at about 1300 km. We cut off our computation therefore at a specified height h_{Lin} for which we take 1100 km and continue from there upwards with a constant temperature gradient. This serves as a very crude method to correct for the unknown b_2 factor at heights up to 1400 km.

C. Lyman Series Losses

For the Lyman series losses one could take, as in the case of the Balmer series, the approximate formula given by Athay (1966b). However the question of the departure coefficient b_1 is much more severe in this case where b_1 ultimately becomes very much larger than b_2. To get a reasonable estimate of the Lyman series losses in spite of this uncertainty about b_1 we had to use information from the observation of the Lyman α line which dominates all other Lyman series losses. Hinteregger (1961) gives a flux of $\pi F_{\text{Ly}} = 2.04 \times 10^5$ erg/cm² s and Detwiler *et al.* (1961) give a flux of $\pi F_{\text{Ly}} = 2.35 \times 10^5$ erg/cm² s at the solar surface. We suppose that the emission of this flux occurs over a height interval of D km, the emission rate rising linearly to a maximum at $D/2$ and falling back to zero linearly again. We have then

$$\frac{d\pi F_{\text{Ly}}}{dh} = \begin{cases} A\left(h - h_{\text{Mid}} + \frac{D}{2}\right) \text{ in } h_{\text{Mid}} - \frac{D}{2} \leqq h \leqq h_{\text{Mid}} \\ A\left(h_{\text{Mid}} - h + \frac{D}{2}\right) \text{ in } h_{\text{Mid}} \leqq h \leqq h_{\text{Mid}} + \frac{D}{2} \end{cases}, \tag{25}$$

where h_{Mid} is the height of the greatest emission and

$$A = \frac{4}{D^2} \pi F_{\text{Ly}}. \tag{26}$$

For D we usually took 5–20 km and for h_{Mid} 1865 to 2200 km see Section 6.

D. The Metallic Line and Bremsstrahlung Losses

For the high temperature region the radiation losses may be computed following Tucker and Gould (1966) with the lines published by Pottasch (1964, 1967). However adding up all XUV line fluxes with shorter wavelength than 1206 Å as given by Hall *et al.* (1963) we find only a radiative flux of 7.4×10^4 erg/cm² s. This may then simply be introduced as a fraction of the Lyman loss in Eq. (25).

Thus the total radiative loss may be written

$$\frac{d\pi F_{\text{Rad}}}{dh} = \frac{d\pi F_{\text{H}^-}}{dh} + \frac{d\pi F_{\text{Ba}}}{dh} + \frac{d\pi F_{\text{Ly}}}{dh} + \frac{d\pi F_{\text{XUV}}}{dh}. \tag{27}$$

4. Thermal Conduction

In the transition layer thermal conduction serves as a most effective means to balance radiative losses. To see the competition of the shock dissipation and thermal conduction it was necessary to compute in detail the coefficient K of thermal conduction from the region of a completely neutral to the region of a fully ionized gas (Ulmschneider, 1969). We have taken the values of this coefficient for a mixture of H and 10 percent He by number. Using thermal conduction as a means to balance radiative losses one has to keep in mind that as we have no external heat reservoir we need to put in ultimately the radiative loss in form of mechanical heating by waves travelling out of the convection zone. Thermal conduction serves simply as a means to transport energy from the shock heated lower corona to the region of Ly α radiation loss. Thus the conductive flux

$$\pi F_{\text{Cond}} = K \frac{dT}{dh} \tag{28}$$

rises rapidly to a maximum and decreases again when shock heating takes over, eventually reaching zero at the height of maximum coronal temperature.

5. Energy Balance and Hydrostatic Equation

In order to construct a theoretical chromospheric model one may neglect at first the influence of the gas flow due to the solar wind. The justification for this is that with an ion flux as mentioned in

Section 2 one may estimate that the heat flux of the solar wind $\varrho u H$ is only about 2×10^4 erg/cm² s. Here $H = 5/2\, RT/\mu$ is the enthalpy and $T = 2 \times 10^6$ °K. The flux due to the kinetic energy of the solar wind is even less than this heat flux. In this case the continuity equation is fulfilled identically and Eulers equation is reduced to the simple hydrostatic equation.

$$\frac{dp}{dh} = -\varrho g . \tag{29}$$

Here p is the pressure, ϱ the density and g the solar gravitational acceleration.

The importance of wave pressure which arises from absorption and reflection of wave momentum may be estimated using

$$\frac{dp_{\text{Wave}}}{dh} = \frac{A}{c}\frac{d\pi F_{\text{Mech}}}{dh} , \tag{30}$$

where A is a value between 1 for pure dissipation and 2 for pure reflection. With the results for πF_{Mech} shown in Fig. 3 we find that the wave pressure gradient is only about 1 percent of the gas pressure gradient. Thus wave pressure may be disregarded in the chromosphere. From Eq. (29), knowing ϱ at a lower point one simply computes p at the higher point.

The temperature is determined by the energy balance equation.

$$\frac{d\pi F_{\text{Mech}}}{dh} + \frac{d\pi F_{\text{Cond}}}{dh} = \frac{d\pi F_{\text{Rad}}}{dh} \tag{31}$$

We have found it necessary to fulfil Eq. (31) very accurately because wrong use of this equation leads to great difficulties.

Ulmschneider (1967) and de Loore (1970) have used this Eq. (31) in the form valid for cases with solar wind flow

$$\frac{dT}{dr} = \frac{r_0}{K_0 T^{5/2} r^2}$$

$$\left\{\text{FLOW} - \text{DISS} + \text{RAD} + \frac{K_0}{r_0} T_0^{5/2}\frac{dT_0}{dr}\right\} . \tag{32}$$

Aside from the fact that the $T^{5/2}$ behavior of the coefficient of thermal conductivity is used, valid only in the fully ionized region, this Eq. (32) is correct. However one has to take great care to use this equation in the lower chromosphere. At these heights the values of the radiative flux RAD and the mechanical flux DISS are by a factor of up to 10^5 greater that the remaining conductive and solar wind fluxes. Equation (32) solves for a small term being the result of the cancellation of two very large terms. In the works of Ulmschneider (1967) and de Loore (1970) these large terms were not properly cancelled and therefore huge temperature gradients resulted.

This difficulty was avoided in Eq. (31) by starting with a balanced initial condition and subsequently balancing this equation to an accuracy of 10^{-8} of the largest term. The procedure to do this was to guess a temperature which overfulfilled Eq. (31) then to search for another temperature which underfulfilled Eq. (31) and finally to use the extremely fast Aitken interpolation scheme (Abramowitz and Stegun, 1964, p. 879). The target accuracy was usually reached by solving Eq. (31) seven times.

This gives the temperature at the higher point. Repeating with the new pressure and temperature the above process we step through the whole atmosphere.

6. Results and Discussion

A. The Chromosphere

Because the acoustic waves suffer radiation losses it is uncertain how much energy finally ends up in a fully developed shock wave at a certain height. We assume that at an initial height for which we take 800 km above $\tau_{5000} = 1$ temperature and pressure are given by an empirical model. This height is some distance away from the temperature minimum such that we may expect shock heating to be the sole heating mechanism. Likewise the departure from LTE for the second hydrogen level is small. This indicates that the Balmer series losses are negligible against H^- losses (see Fig. 3). Taking now the wave period $P = 1/\nu$ as a free parameter we may construct a series of models of different periods by integrating Eqs. (10), (29) and (31). The initial strength of the wave is computed by requiring that shock heating is exactly balanced by radiation loss. The initial shock strength is therefore

$$\bar{\eta} = \left(\frac{12}{\gamma(\gamma+1)p\nu}\frac{d\pi F_{H^-}}{dh}\right)^{1/2} . \tag{33}$$

Integrations performed are shown in Fig. 2 based on the Noyes and Kalkofen (1970) model. It is seen that a wave period P of around 25 s described best the observed temperature versus height relation at heights less than 1400 km. A similar computation using the model of Gingerich *et al.* (1971) shows a wave period of around 30 s. Note that the temperature gradients are constant after 1100 km in order to account for the unknown b_2 factor in the Balmer emission. The decrease of the agreement of theore-

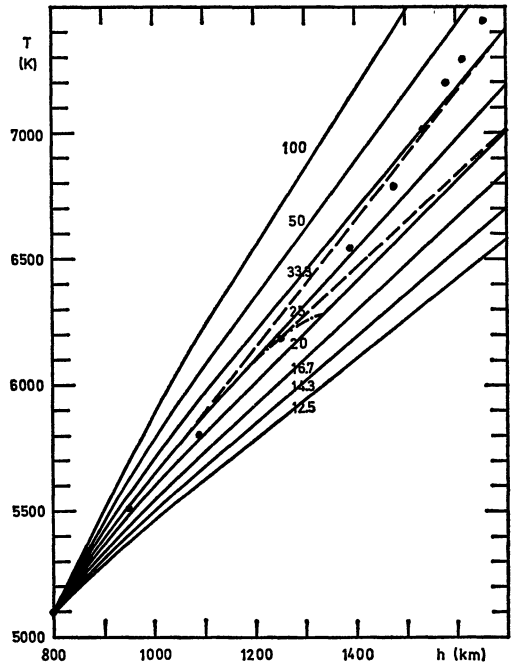

Fig. 2. Temperature T versus height h for theoretical models with the shock wave period as free parameter. Values indicate periods in s. Dots give the observational model of Noyes and Kalkofen (1970). The influence of changing the height of constant temperature gradient is shown dashed. An LTE model is shown dash-point-dashed

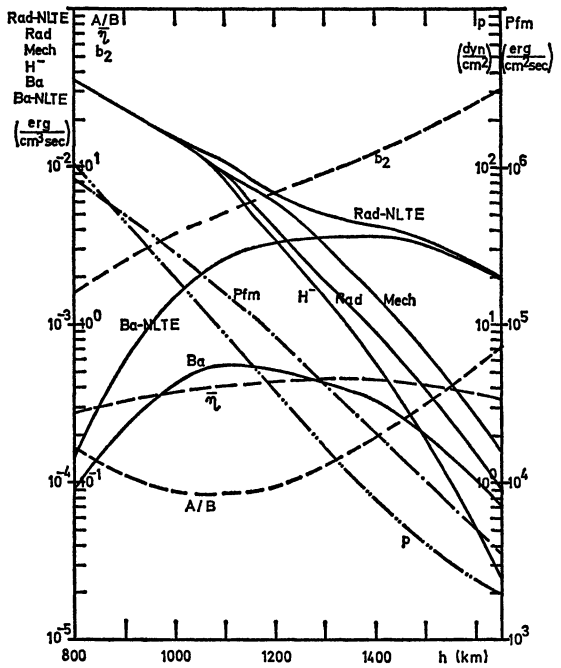

Fig. 3. Total radiation loss (Rad), H^-loss (H^-), Balmer loss (Ba) mechanical heating (Mech), mechanical flux (Pfm), shock strength $\bar{\eta}$, gas pressure p, departure from LTE coefficient b_2 for the second level of hydrogen, non-LTE Balmer losses (Ba-NLTE) and non-LTE radiation loss (Rad-NLTE) as well as the ratio (A/B) of reflection over dissipation in Eq. (10) as function of height h. The model is for a shock wave of 25 s period. The initial point was taken from Noyes and Kalkofen (1970)

tical and observed curves is due to the crudeness of the approximation of the Balmer losses and also to the fact that longer period waves which by now have developed into shocks are not taken into account. The dashed curves in Fig. 2 show the influence of lowering the point at which we continue with a constant temperature gradient. The dash-point-dashed curve in Fig. 2 shows a theoretical model for which the H^- and Balmer losses are in LTE and no adjustment is made for b_2.

In Fig. 3 the total radiation loss (Rad), H^- loss (H^-), Balmer loss (Ba), mechanical heating (Mech), as well as mechanical flux (Pfm), shock strength $\bar{\eta}$ and gas pressure p are shown for a wave with 25 s period and an initial point from Noyes and Kalkofen (1970). It is seen that the shock strength $\bar{\eta}$ is always <1. The curve labelled A/B is the ratio of the first over the second term in Eq. (10). This shows that the reflection part of the mechanical flux loss is much less than the dissipation part which is a consequence of the slow temperature gradient in the chromosphere. It is seen that the total radiation losses (Rad) is balanced exactly by mechanical heating (Mech) up to 1100 km. Because at heights above 1100 km the temperature is fixed by the constant temperature gradient, heating and cooling are not balanced.

In addition we have plotted in Fig. 3 the departure coefficient b_2 taken from Noyes and Kalkofen (1970). The resulting Balmer loss (Ba-NLTE) is shown dashed. This changes the total radiation loss curve into the dashed curve (Rad-NLTE). It is found that this change amounts to an additional flux of 3×10^5 erg/cm^2 s at about 1000 km. As this can be taken out of the shock wave of 25 s period only with difficulty it is suggestive to assume that this flux becomes available for heating by longer period waves which have developed into shock waves in the height interval between 900 and 1000 km.

B. Transition Layer and Constant Conductive Flux Region

The transition layer according to Lyman continuum observations takes place at about 1800 to

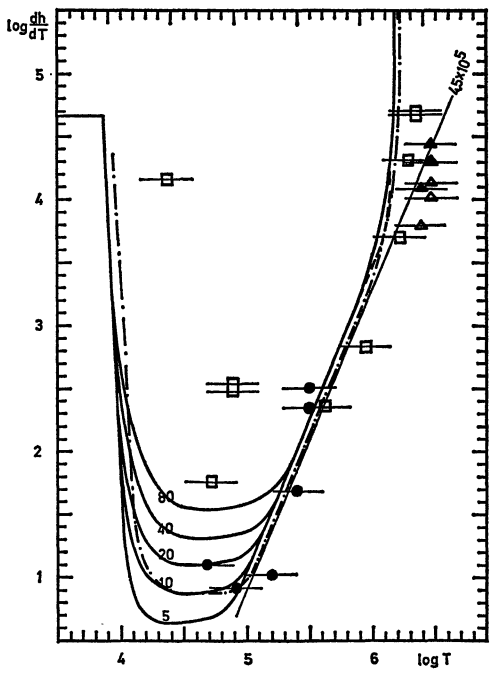

Fig. 4. Inverse temperature gradient $\log \frac{dh}{dT}$ versus temperature $\log T$ for theoretical models with a total Ly α and XUV flux of 3.1×10^5 erg/cm² s. Different models are labelled by the emission interval of Ly α in km. Line observations given by Dupree and Goldberg (1967) are shown. Si lines are shown by rectangles, O lines by circles and Fe lines by triangles. The dash-point-dashed model is an extension of the model of Gingerich *et al.* (1971) with a flux of 4×10^5 erg/cm² s

2200 km (Noyes and Kalkofen, 1970; Gingerich *et al.*, 1971). In Figs. 2 and 3 we have shown that given the right flux and wave period a shock wave may easily balance a radiation loss of a few times 10^{-3} erg/cm³ s in the chromosphere if the energy loss varies not too rapidly with height. In addition to this a lot of mechanical energy becomes available through the shock formation of waves of longer and shorter periods. Thus it might be reasonable to assume that up to the point where the optical thickness of the Lyman α line gets small enough so that strong Lyα losses suddenly occur the radiation losses are still balanced by shock dissipation. The onset of Lyα losses however, through which in a distance D of about 5 to 20 km a flux of 2.5×10^5 erg/cm² s with a peak loss rate of around 5×10^{-1} erg/cm³ s is emitted, is certainly too rapid for shock dissipation.

At this point thermal conduction enters as a means to balance the radiation loss. Figures 4 and 5 show the results for models which start with the initial point of Noyes and Kalkofen (1970), a period of 25 s for the chromospheric shock waves and have a combined Lyα and XUV line flux of 3.1×10^5 erg/cm² s. The height of greatest loss is at 1865 km.

Figure 4 shows the inverse temperature gradient as a function of temperature with XUV line observations given by Dupree and Goldberg (1967). We have however used a different oxygen abundance of $\log A_O = -3.23$ given by Lambert (1968) and a silicon abundance of $\log A_{Si} = -4.45$ given by Lambert and Warner (1968). For the iron abundance we took the values $\log A_{Fe} = -4.40$ given by Garz *et al.* (1970) (open triangles) and $\log A_{Fe} = -4.70$ given by Aller (1970) (filled triangles).

First, the lowest temperature silicon point is far away from the decreasing part of the theoretical curve. This comes from the fact that we have used a constant temperature gradient from 1100 km upwards as an approximation for the Balmer losses. Comparison with the observed temperature behavior (see Fig. 2) shows that actually the temperature gradient is greater at a greater temperature immediately before the Lyα region. This shows that a better treatment of Hα and Lyman continuum losses would bring observation and theory to closer agreement.

Second, models for which the height of the maximum emission is raised to $h_{Mid} = 2200$ km from $h_{Mid} = 1865$ km give exactly the same temperature gradient curve in Fig. 4. This is expected in models of identical conductive flux in a temperature gradient versus temperature plot considering the fact that the coefficient of thermal conductivity is quite insensitive to pressure.

Third, the influence of changing the emission interval D in Eq. (25) on the models is shown in the lower left hand side of Fig. 4. The curves are labelled by the emission interval D in km. It is shown that the smaller the emission interval the larger the temperature gradient. This is in agreement with the expectation that a larger emission rate per cm³ leads to a larger curvature and larger steepness in the temperature versus height curve. Comparing the theoretical curves with the oxygen line observations we conclude that the emission interval is between 5 and 20 km.

Fourth, immediately adjacent to the Lyα region the constant conductive flux region is shown by the straight portion of the models in Fig. 4. With the temperature dependence $K = K_0 T^{5/2}$ of the coefficient of thermal conductivity for a fully ionized gas

Eq. (28) may be written approximately

$$\pi F_{\mathrm{Ly}} + \pi F_{\mathrm{XUV}} = \pi F_{\mathrm{Cond}} = K_0 T^{5/2} \frac{dT}{dh} . \quad (34)$$

Thus we have a $\frac{dT}{dh} \sim T^{-5/2}$ behavior in agreement with observations (Athay, 1966a; Dupree Goldberg, 1967). The best fit of a conductive flux constant temperature profile to the observations is obtained for a flux of 6×10^5 erg/cm² s for the Dupree and Goldberg (1967) abundances. This flux must be reduced as shown in Fig. 4 to about 4.5×10^5 erg/cm² s because of the new oxygen abundance Lambert (1968). The difference between our models with a flux of 3.1×10^5 erg/cm² s and the observed flux amounts to a difference in the silicon abundance of about $\Delta \log A_{\mathrm{Si}} = 0.15$. This is slightly above the uncertainty in the silicon abundance of less than ± 0.10 (Lambert, 1968) combined with the uncertainty in the oxygen abundance of ± 0.05 (Lambert and Warner, 1968). In view of the fact however that these uncertainties are probably overestimated we see a small but significant difference between the theoretical flux and the observed flux which is larger.

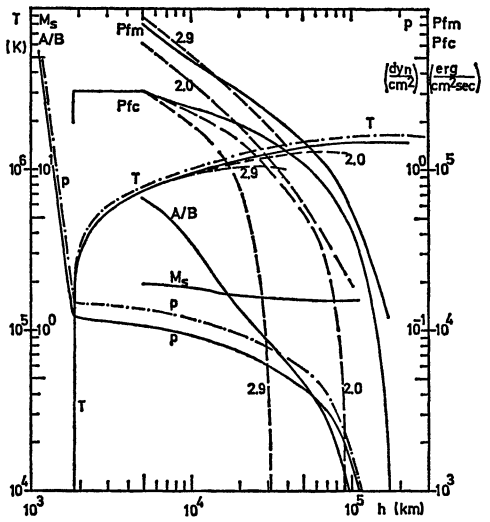

Fig. 5. Temperature T, mechanical flux (Pfm), conductive flux (Pfc), shock Mach number M_s, gas pressure p as well as ratio A/B of reflection over dissipation versus height h. The curves are labelled by the ratio of initial mechanical flux of coronal shock waves over the conductive flux. Dashed curves are for wave periods of 100 s, drawn curves for 200 s. The dash-point-dashed curves give an extension of the model of Gingerich *et al.* (1971)

C. Magnetic Fields and Inhomogeneties

Some of this discrepancy might be taken up by the fact that in a magnetic field the coefficient of thermal conductivity is lowered the more, the greater the angle between flux direction and field line. The consequence of lowering K_0 in Eq. (34) would be a lowering of dh/dT in Fig. 4, that is, the right direction to solve the discrepancy between observational and theoretical values.

Suppose the magnetic field lines are inclined by an angle α to the radial direction then the coefficient of thermal conductivity decreases by a factor of $\cos\alpha$ because of the low thermal conductivity across the field lines. If we assume an angle α of around 30 degrees we would shift our theoretical curve in Fig. 5 downwards by a factor of 1.15 or about $\Delta \log A_{\mathrm{Si}} = 0.05$. Thus a magnetic field inclined at random against the radial direction with an average value of about 30 degrees could close the gap between the theoretical and observed temperature curves.

At this point we want to discuss the influence of magnetic fields on chromospheric heating. For weak shock waves magnetic fields may easily be introduced into the shock equation as shown already by Osterbrock (1961). A comparison of the energy densities of the atmosphere, the acoustic wave and the magnetic field shows however that except at the highest parts of the chromosphere magnetic fields need not to be taken into account if we are not in a plage or sunspot region. As we are interested mainly in the overall behavior of the outer atmosphere of the sun we may disregard active regions as far as the heating of the chromosphere is concerned.

The important question of the influence of the inhomogeneous emission of the XUV lines which is closely connected with magnetic field is presently too difficult to answer.

D. Corona

Finally we want to discuss the coronal region where shock heating replaces thermal conduction. In the absence of any knowledge about the height of shock formation of waves of longer period we arbitrarily select the two heights 5000 and 20000 km at which we introduce a fully developed strong shock wave after Eqs. (11) to (19). The resulting shock dissipation decreases the conductive flux gradually up to the point where the conductive flux and thus the temperature gradient becomes zero, that is the maximum corona temperature is reached. The slow decrease of the conductive flux shortly after the onset of shock dissipation leads to the fact that the

atmosphere is still largely dominated by thermal conduction and thus the exact point of shock formation and whether the wave dissipates in a not yet fully developed manner is not very important. The amount of shock wave flux which has to be introduced at 5000 or 20000 km is a free parameter as well as the frequency of the shock wave. These two parameters have to be chosen carefully however such that the conductive flux becomes zero at some height and that coronal temperatures are reached.

In Fig. 5 we show models which start with the Noyes and Kalkofen (1970) initial point and have a combined Lyα and XUV flux of 3.1×10^5 erg/cm^2 s. The shock wave period of the fully drawn model is 200 s and for the dashed models 100 s. All shocks are introduced at full strength at a height $h_{\rm shock} = 5000$ km and are labelled by the amount of mechanical flux in units of the conductive flux (3.1×10^5 erg/cm^2 s after Eq. (34)). Temperature T, mechanical flux (Pfm), conductive flux (Pfc) as well as the shock Mach number M_s and pressure p are shown. The curve labelled A/B gives the ratio of the reflection to the dissipation term in the strong shock version of Eq. (10). It is seen that due to the large temperature gradient the loss of mechanical flux because of reflection is initially much larger than the loss because of dissipation. Thus the mechanical flux has to be larger than the conductive flux by a factor of between 2.0 and 2.6. The initial shock Mach number for the 200 s period model is $M_s = 1.93$ which corresponds to $\bar{\eta} = 1.40$ indicating a strong shock. This is what we expect from Table 2. The dependence of our theoretical models on the mechanical flux, the wave period, the height of shock formation as well as on the conductive flux may be explained as follows.

First it is seen in Fig. 5 that increasing the mechanical flux input from 2.0 to 2.9 while keeping the wave period constant (100 s) lowers the temperature maximum and shifts it to a lower altitude. This is due to the fact that increased dissipation because of a greater initial mechanical flux reduces the conductive flux much more rapidly leading much faster to the point where the conductive flux becomes zero and the temperature maximum is reached. A further decrease of the initial mechanical flux to the value 1.9 did however yield a model in which the conductive flux is not balanced and which has therefore no temperature maximum. For shock periods of 100 s we thus find that the mechanical flux has to be larger than 1.9 in order to obtain a physical solution.

Table 3. *Extension of the model of Gingerich et al. (1971) into the transition layer and corona*
Temperature T, pressure p, electron pressure p_e and density ϱ are given as function of height h

h (cm)	T (°K)	p (dyn/cm^2)	p_e (dyn/cm^2)	ϱ (g/cm^3)
1.860E+08	8.930E+03	1.518E−01	4.821E−02	1.828E−13
1.861E+08	1.927E+04	1.513E−01	7.566E−02	6.187E−14
1.863E+08	4.509E+04	1.510E−01	7.880E−02	2.525E−14
1.865E+08	7.047E+04	1.509E−01	7.873E−02	1.614E−14
1.867E+08	9.301E+04	1.508E−01	7.869E−02	1.222E−14
1.870E+08	1.183E+05	1.507E−01	7.864E−02	9.603E−15
1.920E+08	2.112E+05	1.494E−01	7.796E−02	5.332E−15
2.020E+08	3.042E+05	1.481E−01	7.727E−02	3.670E−15
2.220E+08	4.032E+05	1.463E−01	7.635E−02	2.735E−15
2.520E+08	4.921E+05	1.443E−01	7.529E−02	2.211E−15
2.920E+08	5.720E+05	1.421E−01	7.412E−02	1.872E−15
3.470E+08	6.449E+05	1.393E−01	7.267E−02	1.628E−15
5.000E+08	7.871E+05	1.331E−01	6.942E−02	1.274E−15
8.000E+08	9.396E+05	1.231E−01	6.422E−02	9.875E−16
1.050E+09	1.027E+06	1.163E−01	6.070E−02	8.535E−16
1.300E+09	1.098E+06	1.105E−01	5.765E−02	7.587E−16
1.800E+09	1.206E+06	1.006E−01	5.249E−02	6.286E−16
2.800E+09	1.333E+06	8.342E−02	4.352E−02	4.716E−16
4.800E+09	1.492E+06	6.030E−02	3.146E−02	3.046E−16
5.800E+09	1.546E+06	5.196E−02	2.711E−02	2.533E−16
1.080E+10	1.620E+06	1.731E−02	9.029E−03	8.054E−17
1.580E+10	1.645E+06	6.289E−03	3.281E−03	2.882E−17
2.080E+10	1.649E+06	2.346E−03	1.224E−03	1.073E−17
2.580E+10	1.642E+06	8.786E−04	4.584E−04	4.032E−18

Second the model with 200 s wave period shows a much higher coronal temperature in spite of the fact that the minimal mechanical flux is larger (2.6). This is due to the slow dissipation rate of the 200 s type shock wave because of which the conductive flux decreases much less rapid.

Third we have plotted in Fig. 4 a model (dashed at $\log T = 6.1$) in which the height at which we introduce a fully developed shock wave was $h_{\text{shock}} = 20000$ km with an initial mechanical flux of 2.4 and a period of 200 s. It is seen that this model does not give a greater coronal temperature than the model which starts with $h_{\text{shock}} = 5000$ km and has an initial mechanical flux of 2.6. This is due to the fact that because the pressure is decreased in the 20000 km model the strength of the shock wave is increased and with it the dissipation.

Fourth in Figs. 4 and 5 (drawn dash-point-dashed) as well as in Table 3 we give an extension of the Gingerich *et al.* (1971) model to higher temperatures. Our initial point is the highest temperature point of their model and we have used a combined Lyα and XUV flux of 4×10^5 erg/cm^2 s, an emission internal of $D = 10$ km at $h_{\text{Mid}} = 1865$ km as well as a period of 200 s for the coronal shock wave in order to be in better agreement with the XUV line observations of Fig. 4. h_{shock} was 5000 km and the (minimal) mechanical flux was 2.5. It is seen that the increased conductive flux increases the coronal temperature. However a full agreement with the iron line observations in Fig. 4 is not expected as these lines are emitted in the hot spots of the corona which are not representative for an overall temperature behavior. The averaged temperature at these heights will therefore be in better agreement with our model computation.

Finally we must state that radiative losses should probably be reintroduced at the point where the conductive flux becomes small, but as the unknown effects of magnetic fields and inhomogeneities of the atmosphere on the dissipation of a strong shock wave as well as the neglect of wave pressure in this region introduce large errors it is at the moment unnecessary to be more accurate.

Acknowledgement. The author wants to thank Dr. M. Scholz of Heidelberg for a helpful discussion on abundances.

Literature

Abramowitz, M., Stegun, I.A. 1964, Handbook of math. functions. Nat. Bureau of Standards, Washington.
Aller, L.H. 1970, I.A.U. Meeting Brighton, England.
Athay, R.G. 1966a, *Ap. J.* **145**, 784.
Athay, R.G. 1966b, *Ap. J.* **146**, 223.
Athay, R.G. 1969, *Solar Phys.* **9**, 51.
Athay, R.G. 1970, *Ap. J.* **161**, 713.
Biermann, L. 1946, *Naturwissenschaften* **33**, 118.
Bird, G.A. 1964, *Ap. J.* **140**, 288.
Burke, P.G., Ormonde, S., Whitaker, W. 1967, *Proc. phys. Soc. London* **92**, 319.
Detwiler, C.R., Garrett, D.L., Purcell, J.D., Tousey, R. 1961, *Ann. Géophys.* **17**, 263.
Dupree, A.K., Goldberg, L. 1967, Solar Phys. **1**, 229.
Garz, T., Richter, J., Holweger, H., Unsöld, A. 1970, *Astr. Astrophys.* **7**, 336.
Gingerich, O. 1964, *S.A.O. Spec. Rep.* **167**, 17.
Gingerich, O., de Jager, C. 1968, *Solar Phys.* **3**, 5.
Gingerich, O., Noyes, R. W., Kalkofen, W., Cuny, Y. 1971, Harvard Smithsonian reference atmosphere, to be published.
Hall, L.A., Damon, K.R., Hinteregger, H.E. 1963, *Space Research* **3**. North-Holland, Amsterdam.
Hines, C.O. 1960, *Can. J. Phys.* **38**, 1441.
Hinteregger, H.E. 1961, *J. geophys. Res.* **66**, 2367.
Jordan, S. 1970, *Ap. J.* **161**, 1189.
Kopp, R.A. 1968, *Air Force Cambridge Res. Lab. Rep.* **4**. Bedford, Mass.
Kuperus, M. 1965, *Rech. astr. Obs. Utrecht* **17**, 1.
Kuperus, M. 1969, *Space Sci. Rev.* **9**, 713.
Lambert, D.L. 1968, *Mon. Not. R. astr. Soc.* **138**, 143.
Lambert, D.L., Warner, B. 1968, *Mon. Not. R. astr. Soc.* **138**, 213.
Landau, L.D., Lifshitz, E.M. 1959, Fluid Mechanics. Pergamon, London.
Loore, C.de 1970, *Astrophys. Space Sci.* **6**, 60.
Ness, N.F. 1968, *A. Rev. Astr. Astrophys.* **6**, 79.
Noyes, R.W., Kalkofen, W. 1970, *Solar Phys.* **15**, 120.
Noyes, R.W., Leighton, R.B. 1963, *Ap. J.* **138**, 631.
Osterbrock, D.E. 1961, *Ap. J.* **134**, 347.
Pottasch, S.R. 1964, *Space Sci. Rev.* **3**, 816.
Pottasch, S.R. 1967, *B.A.N.* **19**, 113.
Stein, R.R. 1968, *Ap. J.* **154**, 297.
Thomas, R.N., Athay, R.G. 1961, Physics of the solar chromosphere. Interscience, New York.
Tucker, W.H., Gould, R.J. 1966, *Ap. J.* **144**, 244.
Uchida, Y. 1963, *Publ. astr. Soc. Japan* **15**, 376.
Ulmschneider, P. 1967, *Z. Astrophys.* **67**, 193.
Ulmschneider, P. 1969, *Astr. Astrophys.* **4**, 144.
Ulmschneider, P. 1970, *Solar Phys.* **12**, 403.

P. Ulmschneider
Astronomisches Institut und Sternwarte
der Universität Würzburg
BRD — 8700 Würzburg,
Büttnerstr. 72, Germany